https://doi.org/10.46813/2023-147-059

STRUCTURE AND MECHANICAL PROPERTIES OF Ti-Cr-Al-Nb AND Ti-Cr-Al-Nb-V MULTICOMPONENT ALLOYS

O.M. Velikodnyi, R.V. Vasilenko, O.S. Kalchenko, I.V. Kolodyi, Y.O. Krainiuk, A.V. Levenets, P.I. Stoev, M.A. Tikhonovsky, G.D. Tolstolutska
National Science Center "Kharkov Institute of Physics and Technology", Kharkiv, Ukraine
E-mail: avlevenets@gmail.com

The empirical and semi-empirical models were used to analyze the phase-structural state of five- and four-component alloys of the Ti-Cr-Al-Nb-V system. Two compositions of lightweight alloys were selected for experimental study: $Ti_{60}Cr_{11}Al_7Nb_{11}V_{11}$ and $Ti_{60}Cr_{11}Al_7Nb_{22}$ (at. %). Ingots of these alloys were obtained by argon-arc melting method, and they were subjected to homogenization, deformation by rolling and subsequent annealing at different temperatures. The influence of annealing temperature on the phase-structural state of the alloys, their hardness, and mechanical properties during tensile tests has been studied experimentally. It was found that the change of phase composition and grain size during annealing in the temperature range of 700…900 ºC practically does not affect the hardness and tensile strength of alloys. Annealing at 900 ºC transforms the alloys into a single-phase state with bcc lattice and significantly increases the elongation to fracture, which is about 30% for both alloys. In addition, the yield strength and tensile strength of the five-component alloy are noticeably higher than those of the four-component alloy.

PACS: 61.50.Ah,62.20.-x,68.37.-d

INTRODUCTION

The development of nuclear energy and its safety depend significantly on the creation of new structural materials that must have improved mechanical properties and corrosion resistance in operation, as well as high radiation resistance. In recent years, along with the improvement of austenitic and ferritic-martensitic reactor steels [1, 2], much attention has been paid to the development and research of a fundamentally new class of radiation-resistant materials – so-called high-entropy or multi-component concentrated alloys [1, 3–6].

Titanium-based alloys are of considerable interest to the nuclear power industry, as they are already used as structural materials for the manufacture of capacitors, steam turbine working blades, heat exchange equipment, and in the production of power fasteners for flange connections and connectors of various technological systems of reactor equipment for nuclear and fusion plants [7–9]. The advantages of titanium alloys are high specific strength, corrosion resistance in various environments, stability of mechanical properties, processability, nuclear properties, and the ability to weld with various types of welding. In recent years, in connection with the development of the latest nuclear power plants with fast neutron reactors, the possibility of using titanium alloys for the manufacture of fuel element cladding is being considered. Fast neutron reactors operate with a liquid metal cooling system. When melts of low-melting heavy metals are used as cooling environment, the main problem is corrosion compatibility and stability of mechanical properties of structural materials in interaction conditions with liquid metals [10, 11]. Lightweight titanium-based multicomponent alloys typically contain aluminum and vanadium in high concentrations, which allows for low densities. Finding a balance between density, mechanical properties, and corrosion resistance of lightweight alloys is a critical issue. To achieve a balance of these properties, it is reasonable to consider four- and five-component titanium alloys containing, in addition to aluminum and vanadium, a significant proportion of chromium, which is a corrosion-resistant element, and niobium, which can improve mechanical properties. Studies have shown that high configurational entropy, which is achieved by using equiatomic ratios of elements, is not a requirement for the formation of solid solutions [12]. This indicates that it is possible to remove the restriction on the equiatomic ratio of a large number of elements in multicomponent alloys. Therefore, non-equiatomic medium-entropy alloys have recently appeared, adding flexibility to the design of new multicomponent alloys [13, 14].

The aim of this work is to develop new multicomponent concentrated alloys based on Ti-Cr-Al-Nb and Ti-Cr-Al-Nb-V systems, which are promising as structural materials, including for nuclear reactors, and to study their structure and mechanical properties.

ALLOY SELECTION, METHODS OF PRODUCTION AND RESEARCH

Selection of alloy composition. According to the objective, it was decided to study an alloy from the above systems that would have a single-phase structure with bcc lattice with increased radiation resistance. Prediction of phase structure formed in alloys of specific elemental composition is extremely important because of numerous possible variants of alloy composition in the presence of 4 and 5 components. Usually, phase composition is determined by the phase diagrams obtained experimentally. This approach is possible for binary and simple ternary system but is hardly implement for complex multicomponent systems with a large range of concentrations. The phase composition can be obtained by calculation using programs such as CALPHAD, but the values of the quantities required for such calculations are not always

known. There are also empirical and semi-empirical rules used to predict the phase composition, which are mostly based on the Hume-Rosery rule and five known factors [15–24]: configurational entropy of mixing, enthalpy of mixing, difference in atomic size of alloy elements, valence electron concentration and electronegativity. There are various criteria based on the ratio of these factors. These criteria are given in Table 1. We have calculated these criteria for a large number of alloys of the Ti-Cr-Al-Nb and Ti-Cr-Al-Nb-V systems. It should be noted that the enthalpies of interaction of different pairs of atoms in the corresponding binary alloys were obtained using the Miedema theory [25]. The analysis of the obtained data, as well as the known data on the flow of each element on the properties of existing titanium alloys, allowed us to select the following alloys for the study: #1 – $Ti_{60}Cr_{11}Al_7Nb_{11}V_{11}$; #2 – $Ti_{60}Cr_{11}Al_7Nb_{22}$. According to most criteria, alloys of this composition should be single-phase and have a single-phase bcc lattice, at least in the high temperature region (Table 2).

Table 1

Criteria for determining the phase composition and crystal lattice of HEA

Criterion A: correlation between ΔS_{mix}, ΔH_{mix}, and δ			
A1	$-15 \le \Delta H_{mix} \le 5$ kJ/mol $0 < \delta < 5$	simple disordered solid solution (SDSS)	[15]
	$-20 \le \Delta H_{mix} \le 0$ kJ/mol $5 < \delta < 6.6$	disordered solid solutions (DSS)	[16]
A2	$-22 \le \Delta H_{mix} \le 7$ kJ/mol $0 \le \delta \le 8.5$ $11 \le \Delta S_{mix} \le 19.5$ J/K·mol	solid solution (SS)	[17]
A3	$-10 \le \Delta H_{mix} \le 5$ kJ/mol $\delta < 4$ $\Delta S_{mix} > 13.38$ J/K·mol	simple solid solution (SSS)	[18]
	$50 \le \Delta H_{mix} \le 0$ kJ/mol $4 \le \delta \le 20$ $4 \le \Delta S_{mix} \le 18$ J/K·mol	amorphous phase (AP)	[19]
Criterion B: correlation between Ω and δ			
B	$\Omega > 1.1$ $\delta < 6.6$	solid solution	[20]
Criterion C: correlation between VEC and δ			
C1	$\delta < 5$	FCC lattice	[21]
	$\delta > 5.4$	BCC lattice	
C2	VEC ≥ 8	FCC lattice	[22]
	VEC < 6.87	BCC lattice	
C3	$4.33 <$ VEC < 7.55	BCC lattice	[23]
	$7.80 <$ VEC < 9.50	FCC lattice	
Criterion D: correlation between $\Delta\chi$ and δ			
D	$0.03 < \Delta\chi < 0.06$ $1 < \delta < 6$	no intermetallic compounds (nC)	[24]
	$\Delta\chi \approx 0.09…0.14$ $\delta \approx 6$	appearance of compounds (intermetallic, σ-phase) (aC)	

ΔH_{mix} – mixing enthalpy; δ – atomic size mismatch; ΔS_{mix} – mixing entropy; Ω – dimensionless parameter; VEC – valence electron concentration; $\Delta\chi$ – electronegativity.

Table 2

Predicted structure of studying alloys: #1 – $Ti_{60}Cr_{11}Al_7Nb_{11}V_{11}$; #2 – $Ti_{60}Cr_{11}Al_7Nb_{22}$

Alloy (x value)/ Criterion	A1	A2	A3	B	C1	C2	C3	D
#1	DSS	TZ	TZ	SS	TZ	BCC	BCC	nC
#2	SDSS	TZ	TZ	SS	FCC	BCC	BCC	nC

TZ – transition zone.

Methods of alloy obtaining and structure and properties investigation. Ingots of the multicomponent alloys were produced by arc melting of the components with a non-consumable tungsten electrode in high-purity argon. Before melting, for additional argon purification, the titanium getter was melted for several minutes. The purities of the alloying elements were higher than 99.9%. To ensure chemical homogeneity, the ingots were flipped over and remelted at least 5 times, and ingots' size was 12×12×30 mm. After that, the homogenization annealing was carried out at 1100 °C for 1 h (in high purity argon), followed by quenching in

the air. After that, ingots were rolled to 0.6 mm with interim annealing at 1100 °C. The specimens for microstructure were produced from the received ingots and tapes by spark cutting.

X-ray diffraction (XRD) patterns of the specimens were recorded using "DRON-4-07" diffractometer equipped with a Bragg-Brentano geometry, a Cu-Kα radiation source, a Ni absorbing filter and a scintillation detector. Standard processing (background removing, Kα2 reduction, diffraction peaks fitting by pseudo-Voigt function) was applied for all diffraction patterns to obtain the peak characteristics (diffraction angle 2θ, integral intensity I, integral breadth B, interplanar spacing d.

Specimens for XRD and microstructure observations were prepared by a standard metallographic process (ground up to #1200 with SiC papers and polished with diamond paste).

To reveal the microstructure, a freshly prepared etchant was used, consisting of 1 part of HNO_3, 1 part of HF, 1 part of H_2O and a few drops of H_2SO_4.

The microstructure of as-cast samples was studied using a metallographic inversion microscope Olympus GX51 and scanning electron microscope JSM 7001F equipped with a system for energy-dispersive X-ray spectroscopy (EDS) INCA ENERGY 350. The fine structure of the samples was studied using a transmission electron microscope JEM-100CX.

The microhardness was measured using a PMT-microhardness tester. The load on the indenter was 200 g, the loading duration was 15 s. The mechanical properties were studied using testing machine INSTRON-5581 under active stretching with speed 10^{-3} s^{-1} at 20 °C. Proportional limit σ_{pr}, tensile strength σ_b and elongation to failure δ were measured. Samples for investigation were in the shape of double blades with working part dimensions of 1×2×10 mm produced by spark cutting along the rolling direction and annealed in a vacuum at different temperatures. The yield strength $\sigma_{0.2}$, tensile strength σ_b and elongation to failure δ were investigated.

RESULTS AND DISCUSSION

Metallographic and electron microscopic investigations. Elemental analysis has shown that the actual composition of as-cast ingots is close to the nominal one (Table 3).

Table 3

Nominal and actual composition (at. %) of studied alloys

Element	Alloy #1, composition		Alloy #2, composition	
	Nominal	Actual	Nominal	Actual
Ti K	60	61.44	60	59.76
Cr K	11	10.89	11	10.53
Al K	7	6.84	7	6.78
Nb L	11	9.96	22	22.93
V K	11	10.87	–	–
Total	100	100	100	100

According to the metallographic investigations, the ingots of both alloys have a coarse-grained structure without visible segregations. When studying the samples rolled and annealed at the same time by scanning electron microscopy, it was found that the microstructure of both alloys when annealed at the same temperatures is almost identical, so we present images for one alloy in the following. After annealing at a temperature of 700 °C, there are precipitations in samples (Fig. 1,a), the amount of which is greater in the alloy with a higher niobium content. After annealing at 800 °C, precipitates are also observed, but their amount is significantly reduced, and their size is increased (see Fig. 1,b). At higher annealing temperatures (900 and 1000 ºC), a coarse crystalline structure without visible emissions is observed, and an increase in the annealing temperature to 1000 ºC leads to a significant increase in grain size, which can reduce strength characteristics. Therefore, for further studies, the maximum annealing temperature was chosen to be 900 ºC, at which the single-phase state is already realized, and the annealing time was reduced to 15 min to reduce the grain size (see Fig. 1,c).

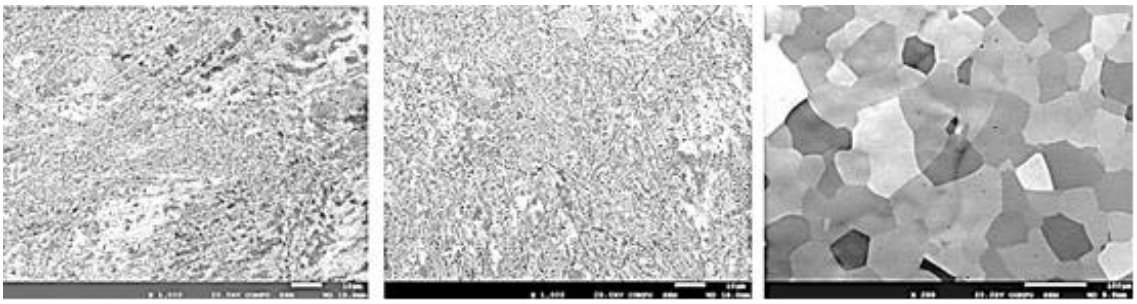

a *b* *c*

Fig. 1. The effect of annealing on the microstructure of $Ti_{60}Cr_{11}Al_7Nb_{22}$ alloy: a – annealing at 700 °C for 1 h; b –- annealing at 800 °C for 1 h; c – annealing at 900 °C for 15 min

For a qualitative study of the elemental composition of the precipitates, we performed mapping, which revealed that the precipitates in both alloys are significantly enriched with chromium, as well as have an increased content of niobium and practically no titanium (Fig. 2). Transmission microscope studies have shown that annealing at 700 °C leads to the onset of recrystallization and the formation of submicron grains (Fig. 3,a,b). With an increase in the annealing temperature to 800 °C, the grain size increases to several microns (see Fig. 3,c,d). As a result of annealing at 900 ºC for 15 min, the average grain size in the $Ti_{60}Cr_{11}Al_7Nb_{11}V_{11}$ alloy was 68 μm, and in the $Ti_{60}Cr_{11}Al_7Nb_{22}$ alloy – 52 μm.

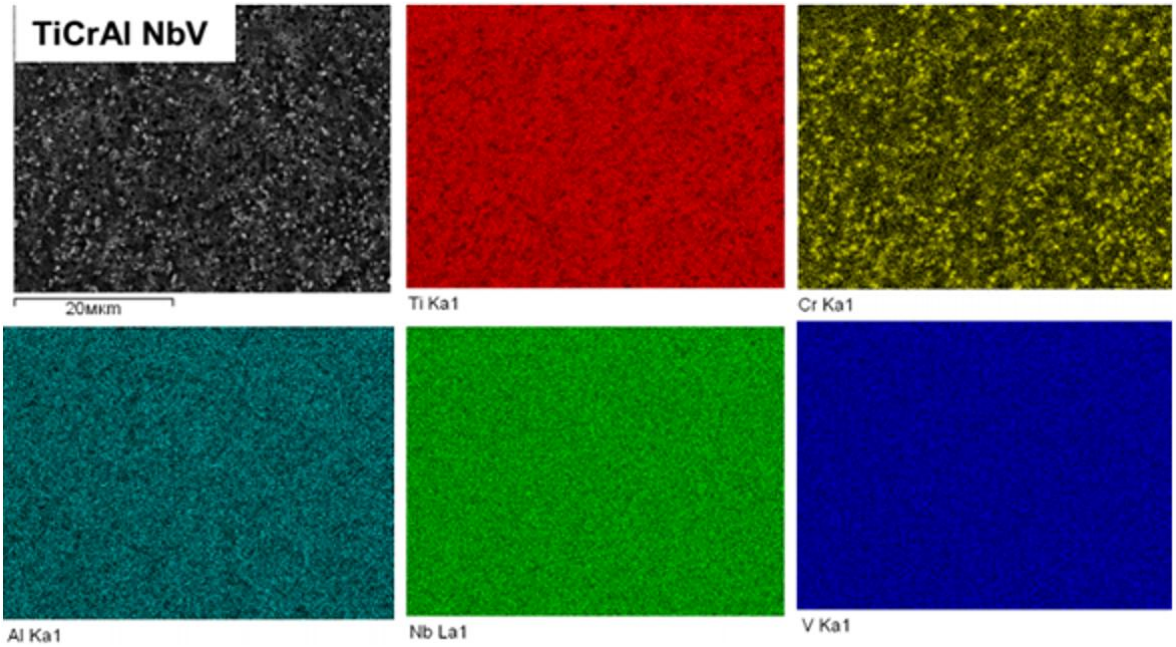

Fig. 2. Elemental distribution in the matrix and precipitations of the $Ti_{60}Cr_{11}Al_7Nb_{11}V_{11}$ alloy after annealing at 800 °C/1 h

X-ray diffraction analysis. X-ray diffractograms of samples are shown in Figs. 4 and 5, and the calculated results are summarized in Table 4. All as-cast samples (see Figs. 4,a, 5,a), marked as #1 and 2, are bcc single-phased. The diffraction lines have a very small half-width, i.e., all samples are in a large-crystal state, which is shown by metallographic studies.

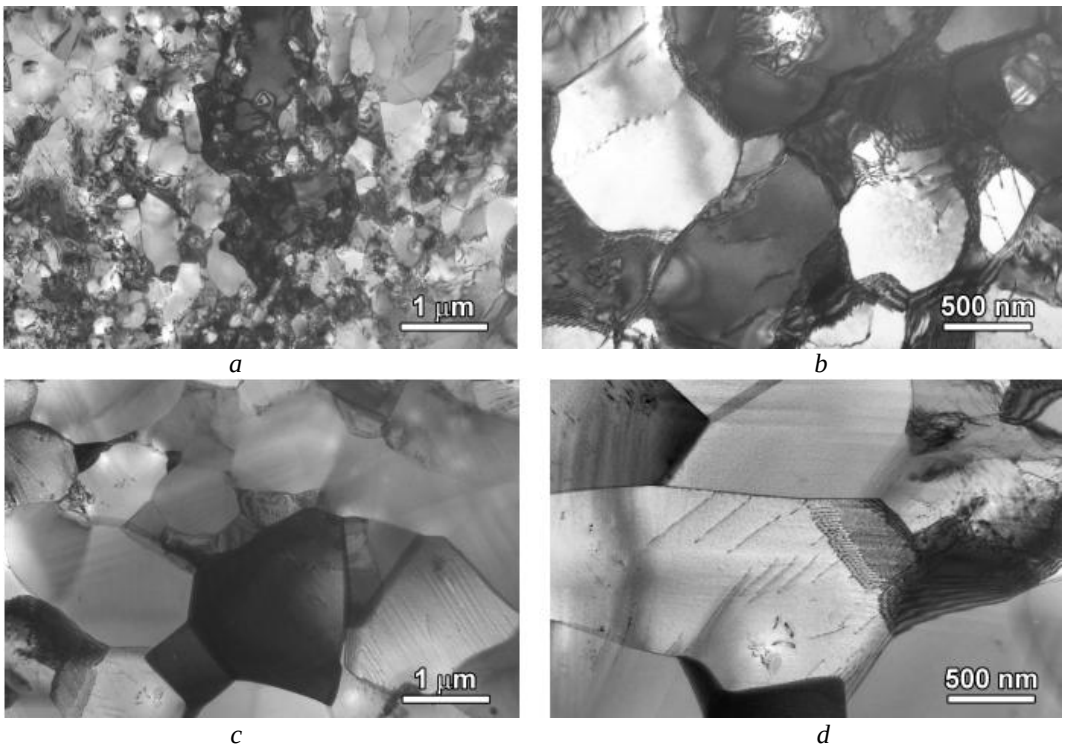

a *b*

c *d*

Fig. 3. The effect of annealing for 1h at 700 °C (a, b) and 800 °C (c, d) on the microstructure of the rolled $Ti_{60}Cr_{11}Al_7Nb_{22}$ alloy

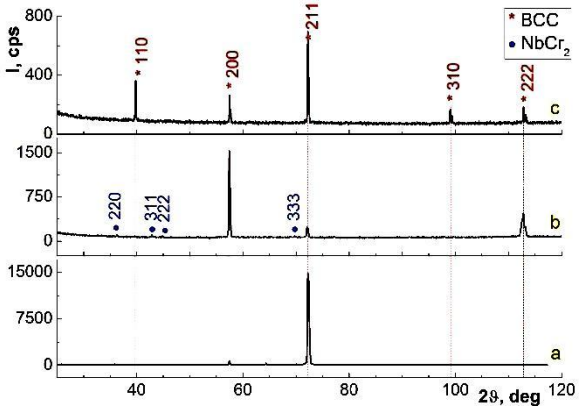

Fig. 4. Diffractograms of $Ti_{60}Cr_{11}Al_7Nb_{11}V_{11}$ alloy: a – as-cast state (#1); b – after annealing 800 °C/1 h (#1.1); c – after annealing 900 °C/15 min (#1.2)

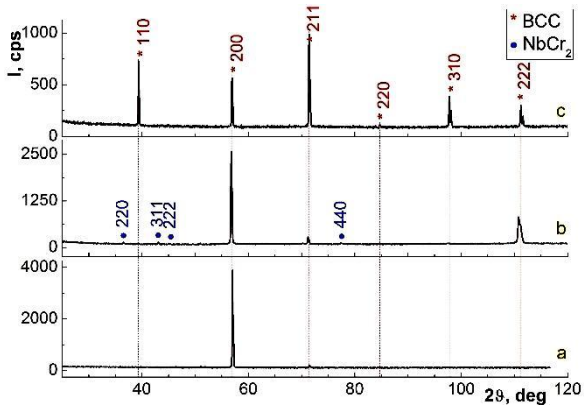

Fig. 5. Diffractograms of $Ti_{60}Cr_{11}Al_7Nb_{22}$ alloy: a – as-cast state (#2); b – after annealing at 800 °C/1 h (#2.1); c – after annealing at 900 °C/15 min (#2.2)

The lattice parameter of the bcc phase increases with the increase in the content of niobium (see Table 4), from a = 3.198 Å for sample #1 to a = 3.230 Å for sample #2, which is associated with the larger size of the niobium atom compared to vanadium (r_V = 1.35Å, r_{Nb} = 1.45 Å).

After annealing at 800 °C for 1 h (see Figs. 4,b, 5,b), the samples (marked as #1.1 and 2.1) also predominantly consist of the bcc phase. However, unlike the as-cast state, the samples also contain imprints of the Laves phase (structural type C15, space group 227), which may be a compound of $NbCr_2$. Analysis of the half-width of the lines showed that these samples are in a coarse crystalline state, and the increased intensity of the diffraction lines (200) indicates the presence of texture (200). The lattice parameter of the bcc phase after annealing at 800 °C increased compared to the initial (as-cast) state (see Table 4). Increasing of lattice parameter of the bcc phase is obviously due to the formation of the $NbCr_2$ Laves phase, namely, due to the transition of a significant part of chromium from the bcc matrix phase to the intermetallic. At the same time, the tendency to increase the lattice parameter with increasing niobium content in the alloy, i.e., in sample #2.1 compared to sample #1.1, remains.

Table 4

Phase composition and lattice parameters of alloys in different states

Sample #	Composition	State	Phase	Lattice parameter a, Å
1	$Ti_{60}Cr_{11}Al_7Nb_{11}V_{11}$	as-cast	bcc	3.198
2	$Ti_{60}Cr_{11}Al_7Nb_{22}$	as-cast	bcc	3.230
1.1	$Ti_{60}Cr_{11}Al_7Nb_{11}V_{11}$	Rolling + annealing at 800 °C/1h	bcc	3.207
			$NbCr_2$	6.998
2.1	$Ti_{60}Cr_{11}Al_7Nb_{22}$	Rolling + annealing at 800 °C/1h	bcc	3.241
			$NbCr_2$	6.959
1.2	$Ti_{60}Cr_{11}Al_7Nb_{11}V_{11}$	Rolling + annealing at 900 °C/1h	bcc	3.203
2.2	$Ti_{60}Cr_{11}Al_7Nb_{22}$	Rolling + annealing at 900 °C/1h	bcc	3.233

Table 5

Microhardness of multicomponent alloys in different states

Microhardness H_μ, MPa	State				
	As-cast	700 °C/ 1h	800 °C/ 1h	900 °C/ 1h	1000 °C/ 1h
$Ti_{60}Cr_{11}Al_7Nb_{11}V_{11}$	2940±27	3030±34	2990±45	3050±28	3090±23
$Ti_{60}Cr_{11}Al_7Nb_{22}$	2820±32	2940±60	2900±24	2910±40	2950±43

After annealing at 900 °C for 15 min (see Figs. 4,c; 5,c), samples are in a single-phase state and consist of the bcc phase. The analysis of the half-widths of the lines showed that all samples are in a coarse crystalline state. The lattice parameter of the bcc phase in both samples increased slightly compared to the initial (as-cast) state. This may be due to the absorption by the samples during annealing of a small amount of residual gases (interstitial elements). At the same time, the tendency to increase the lattice parameter in alloys with increasing niobium content also remains.

Hardness of alloys. The data for microhardness tests of the alloys are presented in Table 5. It can be seen that the structural state of the alloys has little effect

on the microhardness value. We can only discuss certain tendencies. Thus, for two-phase alloys, namely those annealed at 700 and 800 °C, the microhardness slightly decreases with increasing annealing temperature. This may be due to an increase in grain size and formation of the second phase.

In single-phase samples annealed at 900 and 1000 ºC, the pattern is the opposite, that is, the microhardness increases with increasing annealing temperature. The reason for this may be the differences in the degree of ordering processes that are observed in alloys of similar composition [26]. However, additional research is needed to make an accurate conclusion. It should also be noted that the five-component $Ti_{60}Cr_{11}Al_7Nb_{11}V_{11}$ alloy (#1) is slightly harder in all structural states than the four-component $Ti_{60}Cr_{11}Al_7Nb_{22}$ alloy (#2). Nanohardness of the $Ti_{60}Cr_{11}Al_7Nb_{11}V_{11}$ alloy after annealing at 900 ºC for 15 min (samples #1.2 and 2.2 in Table 4) is also higher than that of the $Ti_{60}Cr_{11}Al_7Nb_{22}$ alloy ((4.7 ± 0.07) GPa for sample #1.2 and (4.5 ± 0.18) GPa for sample #2.2). At the same time, the Young's modulus of the five-component alloy is also higher than that of the four-component alloy and is (125.6 ± 3) GPa for sample #1.2 and (122.0 ± 2) GPa for sample #2.2). As shown by measurements in three different zones, the samples have a high degree of homogeneity, which is reflected in a small measurement error (about 3%).

Tensile properties of alloys. Tensile curves for $Ti_{60}Cr_{11}Al_7Nb_{11}V_{11}$ and $Ti_{60}Cr_{11}Al_7Nb_{22}$ alloys in different structural states at testing temperatures of 20 °C are shown in Fig. 6 and the main mechanical parameters obtained from these curves are presented in Table 6.

Electron microscopy studies, and X-ray diffraction analysis showed that, depending on the annealing temperature, there are changes in the phase composition and grain size. However, it should be noted that the measured values of microhardness and tensile strength for the studied alloys is almost unchanged at different annealing temperatures. Particular attention should be paid to the absence of a strengthening effect of submicron and micron precipitations of the $NbCr_2$ Laves phase, which occurred in both alloys at annealing temperatures of 700 and 800 °C.

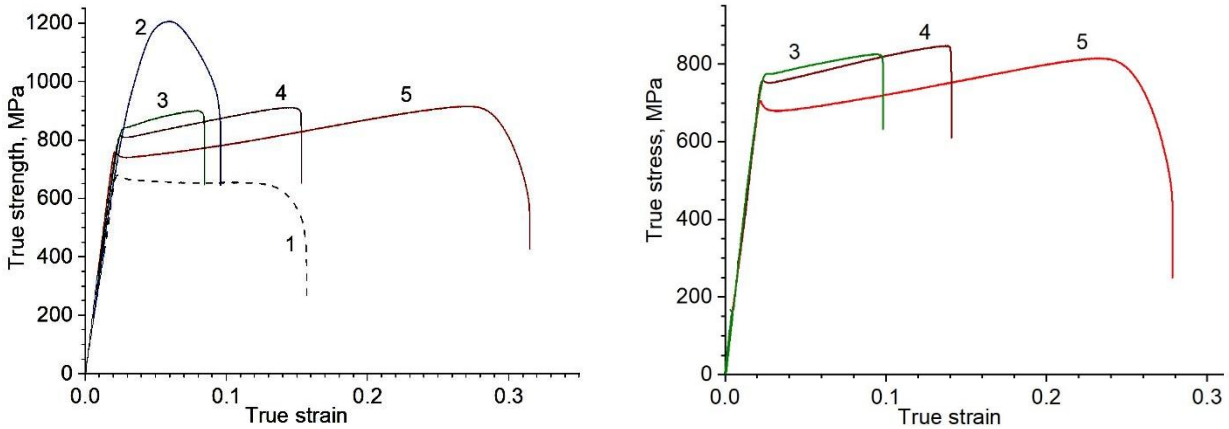

a *b*

Fig. 6. Tensile curves for (a) $Ti_{60}Cr_{11}Al_7Nb_{11}V_{11}$ and (b) $Ti_{60}Cr_{11}Al_7Nb_{22}$ alloys at 20 °C: 1 – as-cast; 2 – rolled; 3 – rolling + annealing at 700 °C/1 h; 4 – rolling + annealing at 800 °C/1 h; 5 – rolling + annealing at 900 °C/15 min

Table 6

Mechanical properties of alloys at 20 °C ($\sigma_{0.2}$ – yield strength; σ_b – tensile strength; δ – elongation to failure

Alloy	Processing	$\sigma_{0.2}$, MPa	σ_b, MPa	δ, %
$Ti_{60}Cr_{11}Al_7Nb_{11}V_{11}$	Rolling	952.7	1206.6	7.5
	Rolling + annealing at 700 °C/1 h	848.7	900.1	6.8
	Rolling + annealing at 800 °C/1 h	813	910.5	13.4
	Rolling + annealing at 900 °C/15 min	760	916.2	30.3
$Ti_{60}Cr_{11}Al_7Nb_{22}$	Rolling + annealing at 700 °C/1 h	771.5	825.5	8
	Rolling + annealing at 800 °C/1 h	755.5	846.7	12.3
	Rolling + annealing at 900 °C/15 min	702.2	815.4	27.1

At the same time, the yield strength decreases with increasing annealing temperature, albeit slowly. The most significant effect of annealing is on the alloy ductility, which increases significantly with increasing annealing temperature. The plasticity of the samples annealed at 900 °C is about 30%, which is considerably higher than that of known high-strength commercial titanium alloys. It is also worth noting that the yield strength and tensile strength of the $Ti_{60}Cr_{11}Al_7Nb_{11}V_{11}$ alloy is higher than that of the four-component $Ti_{60}Cr_{11}Al_7Nb_{22}$ alloy. This correlates with the hardness ratio of these alloys (see Tables 5, 6). It is worth mentioning the ability of the $Ti_{60}Cr_{11}Al_7Nb_{11}V_{11}$ alloy to significantly harden during rolling deformation. Although hardening (the difference between yield strength and tensile strength) at 30% deformation is

about 20% during tensile tests (see Table 6), rolling with a strain rate of 40% leads to an increase in tensile strength by almost 60%.

The fracture surfaces of the studied alloy samples were examined and found to have a pitted pattern specific to plastic failure (Fig. 7). Although the surface structure for both alloys is similar, it can be noted that in the $Ti_{60}Cr_{11}Al_7Nb_{11}V_{11}$ alloy, the pits are smaller, and their size distribution is more uniform. This may be due to the greater structural homogeneity of this alloy, which leads to the greater ductility compared to the $Ti_{60}Cr_{11}Al_7Nb_{22}$ alloy (see Table 6).

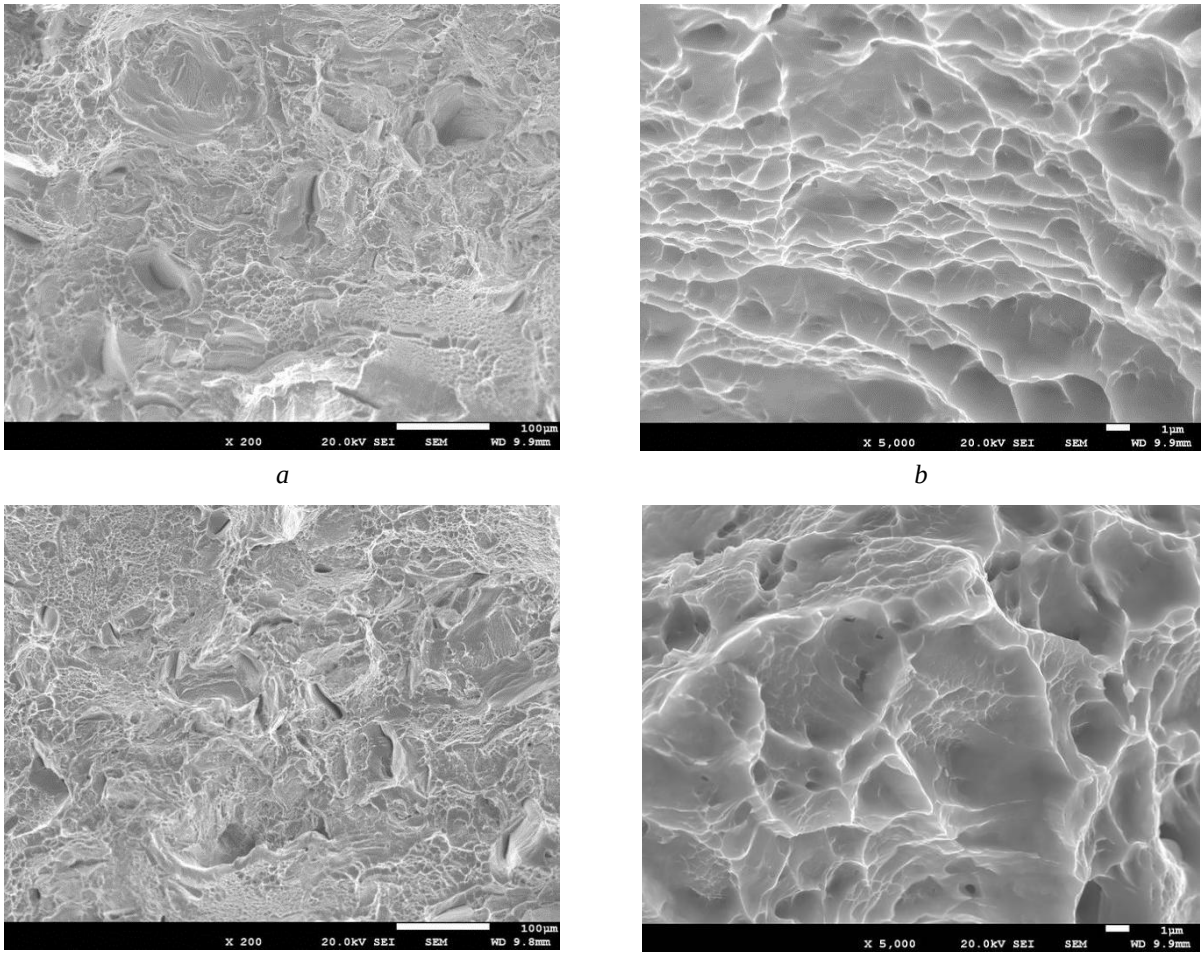

a *b*

c *d*

Fig. 7. The fracture surface of the studied alloys obtained after tensile tests at different magnifications: a, b – $Ti_{60}Cr_{11}Al_7Nb_{11}V_{11}$; c, d – $Ti_{60}Cr_{11}Al_7Nb_{22}$

CONCLUSIONS

1. New lightweight (calculated density 4.95…5.59 g/cm^3) alloys based on the multicomponent Ti-Cr-Al-Nb-V system were developed and studied. Using optical and electron microscopy, as well as X-ray diffraction analysis, it was found that the $Ti_{60}Cr_{11}Al_7Nb_{11}V_{11}$ and $Ti_{60}Cr_{11}Al_7Nb_{22}$ alloys (composition is given in at. %) are single-phase and have a bcc lattice after annealing at temperatures of 900 °C and above. Submicron and micron precipitations of the $NbCr_2$ phase (phase C15) are present in the matrix after annealing at temperatures of 700 and 800 °C.

2. The mechanical properties of the alloys (elastic modulus, microhardness and nanohardness, strength parameters and ductility) were determined in different structural states at room temperature. It is established that presence of C15 phase has hardly any effect on hardness and strength of alloys.

3. It is determined that in single-phase state (after annealing at 900 °C for 15 min) the alloys have high plasticity. Five-component alloy $Ti_{60}Cr_{11}Al_7Nb_{11}V_{11}$ possesses higher mechanical properties in comparison with four-component alloy $Ti_{60}Cr_{11}Al_7Nb_{22}$: yield strength of this alloy is 760 MPa, and elongation to fracture is more than 30%.

4. The combination of low density, high ductility and high yield strength allows us to hope that alloys of this class can find application in various fields of technology, including the creation of new generation nuclear reactors. However, to determine the prospects of these materials, it is necessary to conduct a wide range of studies, including further optimization of the composition, mechanical tests at elevated temperatures, studies of radiation resistance and corrosion behavior in various environments, etc.

ACKNOWLEDGEMENTS

This work was prepared within the project № 2020.02/0327 "Fundamental aspects of the new materials creation with unique physical, mechanical and radiation properties based on the concentrated

multicomponent alloys", implemented with the financial support of the National Research Foundation of Ukraine.

REFERENCES

1. V.N. Voyevodin, G.D. Tolstolutskaya, M. Tikhonovsky, A.S. Kuprin, A. Kalchenko. Mechanisms of radiation damage and development of structural materials for operating and advanced nuclear reactors // *Problems of Atomic Science and Technology*. 2021, N 5(135), p. 3-20; doi:10.46813/2021-135-003

2. Victor N. Voyevodin, Mikhail A. Tikhonovsky, Hanna Yu. Rostova. A new approach to thermo-mechanical treatment of steel T91 by multiple upsetting-extrusion in a ferritic range // *Materials Science and Engineering: A.* 2021, v. 822, p. 141686; DOI: 10.1016/j.msea.2021.141686

3. D.B. Miracle. High entropy alloys as a bold step forward in alloy development // *Nature Communications*. 2019, N 10, p. 1805; DOI:10.1038/s41467-019-09700-1

4. A.V. Levenets, M.A. Tikhonovsky, V.N. Voyevodin, A.G. Shepelev, O.V. Nemashkalo. High-entropy alloys as a prospective class of new radiation-tolerant materials. Research development analysis based on the information databases // *Problems of Atomic Science and Technology*. 2021, N 2(132), p. 3-15; DOI:10.46813/2021-132-003

5. V.N. Voyevodin, S.A. Karpov, G.D. Tolstolutskaya, M.A. Tikhonovsky, A.N. Velikodnyi, I.E. Kopanets, et al. Effect of irradiation on microstructure and hardening of Cr-Fe-Ni-Mn high entropy alloy and its strengthened version // *Phil. Mag*. 2020, N 100(7), p. 822-836. DOI:10.1080/14786435.2019.1704091

6. E. Pickering, A. Carruther, P. Barron, S. Middleburgh, D. Armstrong, A. Gandy. High-Entropy Alloys for Advanced Nuclear Applications *// Entropy*. 2021, N 23(98); DOI:10.3390/e23010098

7. А.М. Паршин, О.Э. Муратов. О применении титановых сплавов для корпусов водо-водяных реакторов // *Вопросы атомной науки и техники. Серия «Физика радиационных повреждений и радиационное материаловедение».* 2005, №3(86), с. 179-181.

8. С.С. Ушков, О.А. Кожевников. Опыт применения и значение титановых сплавов для развития атомной энергетики России // *Вопросы материаловедения*. 2009, №3(59), с. 172-187.

9. Б.Е. Патон, Н.П. Тригуб, С.В. Ахонин. Перспективы использования титана в атомной энергетике Украины // *Современная электрометаллургия*. 2006, №2, с. 23-26.

10. Г.М. Грязнов, В.А. Евтихин, И.Е. Люблинский и др. *Материаловедение жидкометаллических систем термоядерных реакторов*. М.: «Энергоатомиздат», 1989, 222 с.

11. G. Muller, A. Heinzel, J. Konys, et al. Results of steel corrosion tests in Flowing liquid Pb/Bi at 420–600 °C after 2000 h // *Journal of Nuclear Materials*. 2002, N 301, p. 40-46; DOI:10.1016/S0022-3115(01)00725-5

12. Y. Wang, B. Li, H. Fu. Solid solution or intermetallics in a high-entropy alloy // *Adv. Eng. Mater*. 2009, N 11(8), p. 641-644; DOI:10.1002/adem.200900057

13. Y. Deng, C. Tasan, K. Pradeep, H. Springer, A. Kostka, D. Raabe. Design of a twinning-induced plasticity high entropy alloy // *Acta Mater*. 2015, N 94, p. 124-133; DOI:10.1016/j.actamat.2015.04.014

14. Z. Xu, Z. Ma, M. Wang, Y. Chen, Y. Tan, X. Cheng. Design of novel low-density refractory high entropy alloys for high-temperature applications // *Mater. Sci. Eng. A*. 2019, N 755, p. 318-322; DOI:10.1016/j.msea.2019.03.054

15. Y.F. Ye, Q. Wang, J. Lu, C.T. Liu, and Y. Yang. High-Entropy Alloy: Challenges and Prospects // *Materials Today*. 2016, N 19(6), p. 349-62; DOI:10.1016/j.mattod.2015.11.026

16. Y. Zhang, Y.J. Zhou, J.P. Lin, G.L. Chen, P.K. Liaw. Solid-solution phase formation rules for multi-component alloys // *Adv. Eng. Mater*. 2008, N 10(6), p. 534-8; DOI:10.1002/adem.200700240

17. S. Guo and C.T. Liu. Phase Stability in High Entropy Alloys: Formation of Solid-Solution Phase or Amorphous Phase. // *Progress in Natural Science: Materials International*. 2011, v. 21(6), p. 433-46. DOI:10.1016/S1002-0071(12)60080-X

18. Y. Zhang, Ting Ting, Zhi Tang, Michael C. Gao, Karin A. Dahmen, Peter K. Liaw, and Zhao Ping. Microstructures and Properties of High-Entropy Alloys // *Progress in Materials Science*. 2014, N 61, p. 1-93; DOI:10.1016/j.pmatsci.2013.10.001

19. T.S. Srivatsan, Manoj Gupta. *High entropy alloys: innovations, advances, and applications*. CRC Press, 2020.

20. X. Yang, Y. Zhang. Prediction of high-entropy stabilized solid-solution in multi-component alloys // *Materials Chemistry and Physics*. 2012, N 132(2-3), p. 233-238; DOI:10.1016/j.matchemphys.2011.11.021

21. S. Tripathy, Gaurav Gupta, Sandip Ghosh Chowdhury. High Entropy Alloys: Criteria for Stable Structure // *Metallurgical and Materials Transactions: A.* 2018, N 49(1), p. 7-17; DOI:10.1007/s11661-017-4388-z

22. S. Guo, C. Ng, J. Lu, and C.T. Liu. Effect of valence electron concentration on stability of fcc or bcc phase in high entropy alloys // *Journal of Applied Physics*. 2011, v. 109, p. 103505; DOI:10.1063/1.3587228

23. F. Tian, Lajos K. Varga, Nanxian Chen, Jiang Shen, and Levente Vitos. Empirical Design of Single-Phase High-Entropy Alloys with High Hardness // *Intermetallics*. 2015, v. 58, p. 1-6; DOI:10.1016/j.intermet.2014.10.010

24. M.G. Poletti, L. Battezzati. Electronic and thermodynamic criteria for the occurrence of high entropy alloys in metallic systems // *Acta Materialia*. 2014, v. 75, p. 297-306; DOI:10.1016/j.actamat.2014.04.033

25. A.R. Miedema, P.F. de Châtel, and F.R. de Boer. Cohesion in alloys-Fundamentals of a semi-empirical model // *Physica B+C.* 1980, v. 100, N 1, p. 1-28; DOI: 10.1016/0378-4363(80)90054-6

26. G.S. Zherebtsov, N. Yurchenko, E. Panina, M. Tikhonovsky, N. Stepanov. Gum-like mechanical behavior of a partially ordered Al5Nb24Ti40V5Zr26 high entropy alloy // *Intermetallics*. 2020, v. 116, p. 106652; DOI: 10.1016/j.intermet.2019.106652

Article received 12.09.2023

СТРУКТУРА ТА МЕХАНІЧНІ ВЛАСТИВОСТІ БАГАТОКОМПОНЕНТНИХ СПЛАВІВ Ti-Cr-Al-Nb ТА Ti-Cr-Al-Nb-V

О.М. Великодний, Р.В. Василенко, О.С. Кальченко, І.В. Колодій, Є.О. Крайнюк, А.В. Левенець, П.І. Стоєв, М.А. Тихоновський, Г.Д. Толстолуцька

Було проаналізовано структурно-фазовий стан чотирьох- та п’ятикомпонентних сплавів системи Ti-Cr-Al-Nb-V за допомогою емпіричних та напівемпіричних моделей. Для експериментальних досліджень було обрано легкі сплави двох складів: $Ti_{60}Cr_{11}Al_7Nb_{11}V_{11}$ та $Ti_{60}Cr_{11}Al_7Nb_{22}$ (в ат. %). Зливки цих сплавів були виготовлені аргоно-дуговим способом плавлення і піддавалися гомогенізації, деформуванню прокаткою і подальшому відпалу при різних температурах. Експериментально вивчено вплив температури відпалювання на фазово-структурний стан сплавів, твердість та механічні властивості при випробуваннях на розтяг. Встановлено, що зміна фазового складу та розміру зерна при відпалу в температурній області 700…900 ºС практично не впливає на твердість та міцність сплавів. Після відпалу при 900 °С сплави знаходяться в однофазному стані, мають ОЦК-гратку і високу пластичність близько 30%. При цьому, п'ятикомпонентний сплав має вищі механічні властивості порівняно з чотирикомпонентним сплавом.